Bulletin of the Seismological Society of America, Vol. 87, No. 4, pp. 1024–1034, August 1997

Northridge Aftershocks, a Source Study with TERRAscope Data

by Xi J. Song and Donald V. Helmberger

Abstract Broadband and long-period displacement waveforms from a selection of Northridge aftershocks recorded by the TERRAscope array are modeled to study source characteristics. Source mechanisms and moments are determined with long-period data using an algorithm developed by Zhao and Helmberger (1994). These results are compared with those by Hauksson *et al.* (1995) and Thio and Kanamori (1996). The width of the direct pulses at the nearest stations PAS and CALB are measured as indications of the source duration. Another measurement of the source-time functions of these earthquakes is obtained by comparing the short-period to long-period energy ratio in the data to that in the synthetics. These measurements are used to estimate the relative stress drop using a formula given by Cohn *et al.* (1982). The depth distribution of the relative stress drops indicates that the largest stress drops are in the depth range of 5 to 15 km for an aftershock population of 24 events. A correlation of extended surface wave train with source depth is demonstrated for paths crossing the San Fernando basin.

Introduction

The stress field and faulting in the Northridge area is of great importance to the understanding of the tectonics associated with the Transverse Ranges (Fig. 1). Since most of the recorded earthquakes in this area occurred with no surface rupture, their source mechanisms provide essential information for the association of these earthquakes with certain known faults and to the identification of unknown faults (Hauksson *et al.,* 1995). Several studies have been carried out on the Northridge event and its aftershocks. For example, Thio and Kanamori (1996) used surface waves (period 10 to 40 sec) to study the source mechanism, depth, and seismic moment of these earthquakes with a moment-tensor inversion technique (Thio and Kanamori, 1996). With first-motion data from the Southern California Seismic Network, Hauksson *et al.* (1995) compiled a complete report of the source mechanisms, depths, and local magnitudes of the Northridge sequence. Thio and Kanamori's (1996) solutions include many strike-slip and normal faulting, while, in contrast, Hauksson *et al.*'s (1995) results show predominant thrust faulting. When the source mechanism results of the two studies agree, their depth estimates are similar. This is true for about half of the population. For the other half, the depth estimates by the two studies differ by an average of ± 5 km, and the source mechanism results are distinctive from each other. One such example is shown in Figure 2. For this event (number 0415), Hauksson *et al.*'s (1995) source mechanism solution is a thrust (strike 110, dip 55, rake 110) at a depth of 9 km, and Thio and Kanamori's (1996) is a strike slip (231, 31, 1) at a depth of 5 km. While Thio and Kanamori's (1996) result predicts the amplitude well, it fails to fit the P_{nl} waveforms, especially at station GSC. Since Hauksson *et al.*'s (1995) solution is based on P waves, we should expect the P_{nl} wave train to fit better, which it does in this example. Given this type of discrepancy, we model the complete waveforms to check on the mechanisms, depths, and to determine the effective source-time histories to be used in stress-drop estimations. We also discuss the effects of the San Fernando basin on the propagation of the seismic energy along particular paths crossing the basin.

Data and Method

We choose to use Zhao and Helmberger's (1994) grid-search approach to estimate source mechanism and seismic moment. This method matches observed seismograms against synthetics over discrete wave trains and allows relative time shifts between individual wave trains, for example, the P_{nl} wave train and the Rayleigh wave. This allows a better correlation between data and synthetic waveforms and desensitizes the source-mechanism result to the crustal model used to generate the synthetics (Zhao and Helmberger, 1994; Zhu and Helmberger, 1995). Source depth is determined by cycling through different values (5, 8, 11, 14, 17, and 20 km).

With this method, we studied 24 aftershocks with M_L in the range of 4.0 to 5.6. These events are large enough to be recorded at the regional stations with high signal-to-noise ratio. For some of the small events, broadband data are noisy but long-period data are reliable. In our source estimation

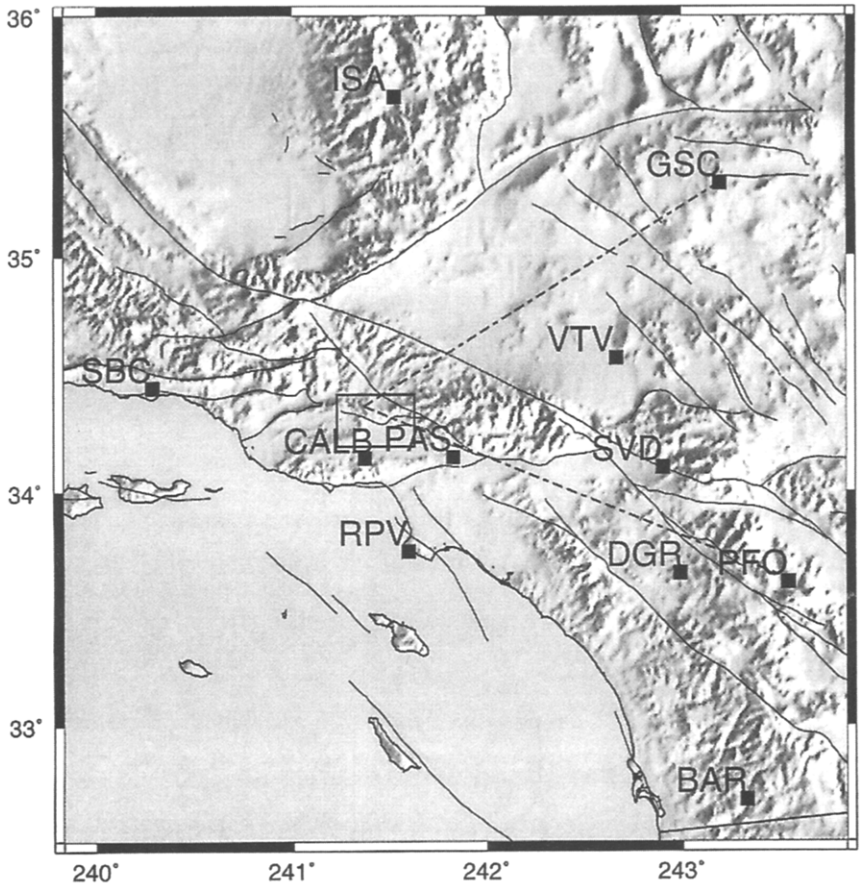

Figure 1. Map of southern California showing TERRAscope stations (solid squares) used in this study and topographic features. The box indicates the Northridge area.

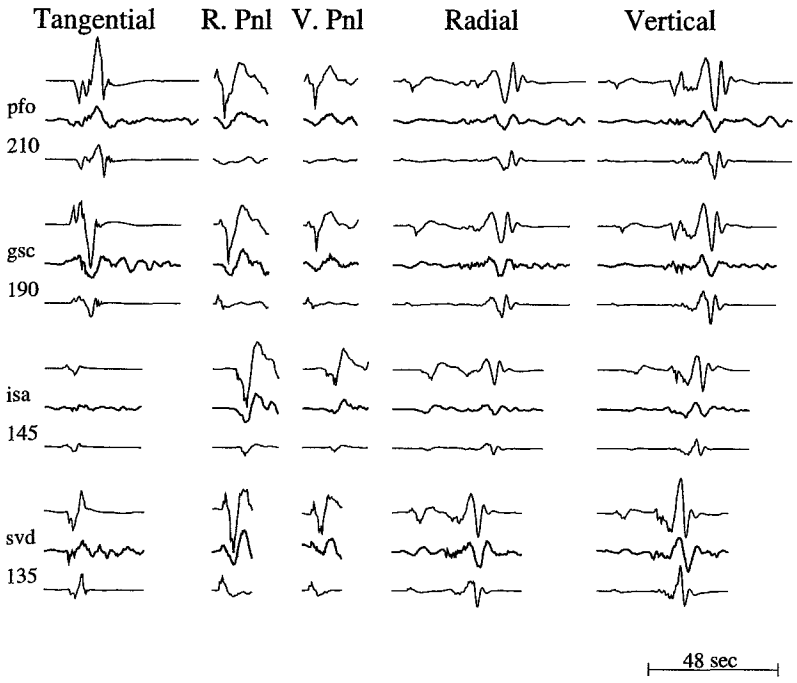

Figure 2. Comparison of data (heavy traces) and synthetics (light traces) for event 0415, after convolving with a long-period Press–Ewing instrument response. The top traces are synthetics with Hauksson *et al.*'s (1995) mechanism and depth. A moment of 1.0 $\times$ 10^{23} dyne·cm (corresponding to a local magnitude of M_L = 4.6) is used for this solution. Seismograms at the bottom of each group are synthetics with Thio and Kanamori's (1996) source mechanism, depth, and moment. Station name and epicentral distances are given. All seismograms for the same station are scaled by amplitude, with the P_{nl} waves blown up and shown separately. A triangular far-field source-time function with a duration of 0.4 sec is used. A small time shift is used to align synthetics with data.

process, we apply a long-period Press-Ewing (LP3090) instrument response on both data and synthetics for all events studied to obtain stable long-period estimates of M_0. We use Green's functions generated by Dreger (1992) for the standard southern California model, using a reflectivity method (Fuchs and Muller, 1971; Bouchon, 1981; Saikia, 1994). An example of the fit between data and synthetics determined by this procedure is shown in Figure 3. The P_{nl} waves and Rayleigh waves are fit well, but the Love-wave data are more complicated than corresponding synthetics.

It is usually difficult to retrieve the source-time history by matching a set of synthetics to broadband seismograms, since many stations have some high-frequency ringing, such as station SVD (Fig. 4). A relatively simple procedure is to equalize the energy content in different frequency band between data and synthetics (Zhao and Helmberger, 1996; Jones and Helmberger, 1996). We apply the Wood–Anderson short-period instrument response (WASP) to both data and synthetics in order to compute the short-period energy. To obtain an estimate of the source-time history, we match the short-period (WASP) to long-period (LP3090) energy ratio in the observed P_{nl} wave train to synthetics. Symmetric trapezoidal source-time functions are assumed. Figure 4 displays the broadband data and the synthetics with this far-field source-time function, and the source mechanism determined with the long-period data (Fig. 3). In this example, a (0.2, 0.2 sec) triangle fits the best, that is, a source duration of 0.4 sec. Note the match of the frequency content in the data and synthetics, especially for the P_{nl} wave train.

A more traditional and straightforward estimate of the source duration can be obtained by measuring the width of the direct pulse at local stations (e.g., Hardebeck and Hauksson, 1996). Many of the aftershocks were recorded at stations PAS and CALB, with source-receiver distances less than 50 km. Figure 5 displays some of the direct P-wave pulses recorded at these two stations from which we were able to measure the source durations. For events shown in this figure, we get similar results at PAS and CALB, although there is some variation of the pulse width between these two stations. For other events in the data set, especially large events and those with complex sources (Fig. 6), we were not able to apply this kind of measurement. However, for those events to which both Zhao and Helmberger's (1996) energy ratio method and the direct measurement can be applied, a good correlation exists between the two measurements (Fig. 7), except for an offset. The offset is expected because the synthetics in Figure 4 do not contain scattering as the data do. For the purpose of obtaining relative source duration

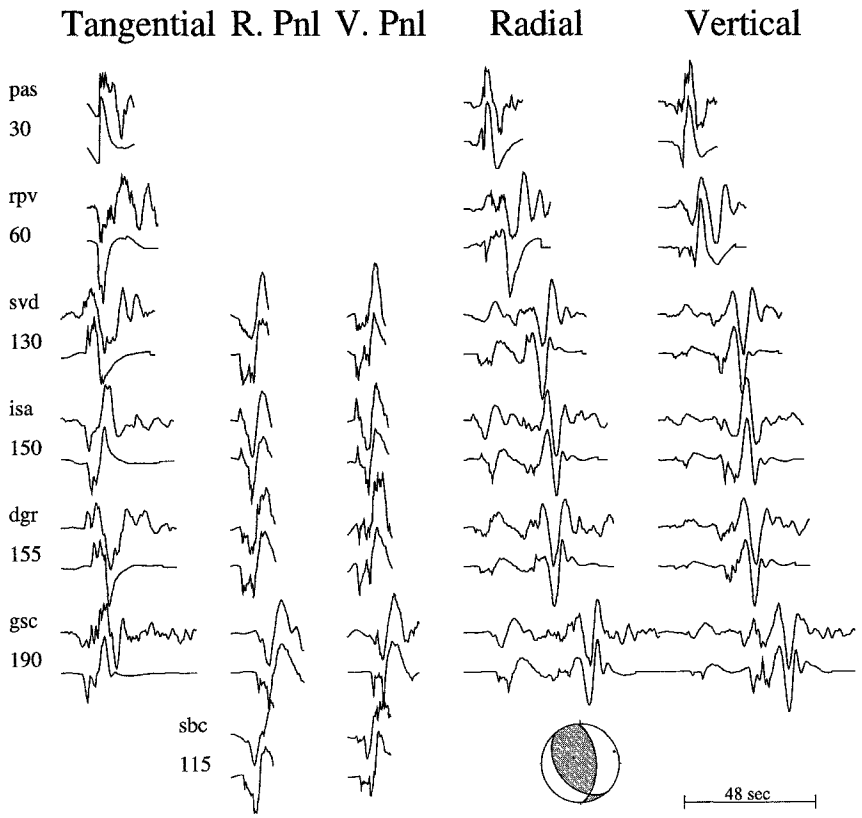

Figure 3. Comparison of long-period displacement data (event 1839) and corresponding synthetics for the mechanism displayed, as determined with the grid-search method ($M_0 = 8.5 \times 10^{22}$ dyne·cm). A source depth of 14 km and a triangular far-field source-time function with a duration of 0.4 sec are used. All seismograms are scaled to unit height. There is a 25% standard variation for the seismic moment.

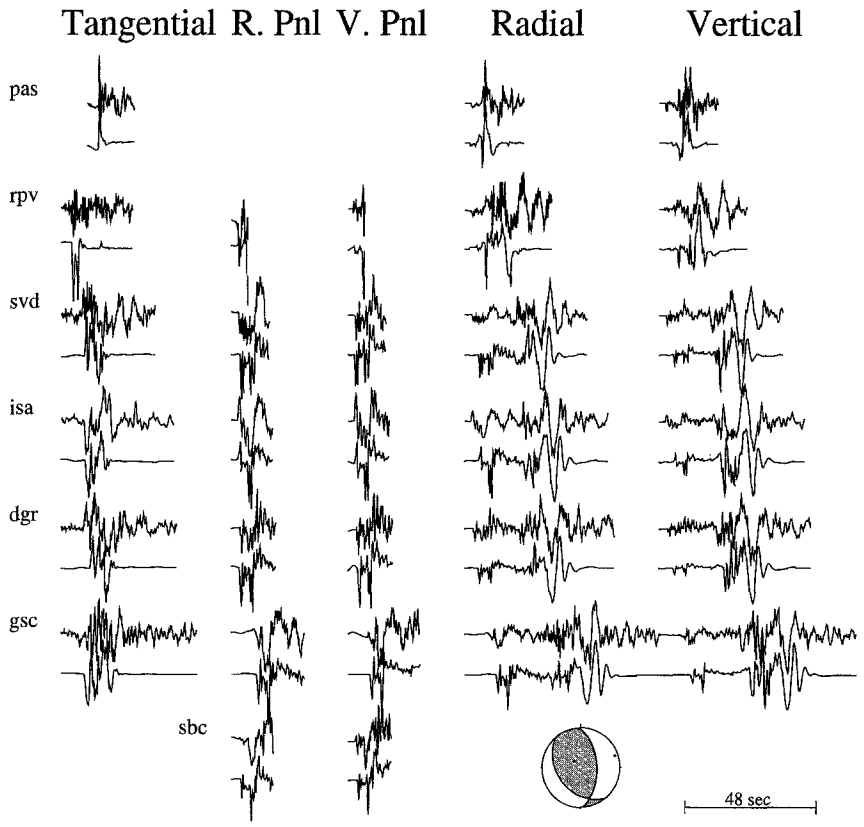

Figure 4. Comparison of broadband displacement data (event 1839) and corresponding synthetics for the mechanism displayed in Figure 3.

from event to event, Zhao and Helmberger's (1996) method appears to be a good alternative to the direct measurement, since path scattering properties should be nearly constant.

To measure the stress drop of an earthquake, many researchers (e.g., Cohn *et al.,* 1982; Jones, 1995) have used the empirical formula

$$\Delta\sigma(\text{bar}) = \frac{1.84 \times 10^{-22} M_0(\text{dyne}\cdot\text{cm})}{\tau^3\ (\text{sec})}, \qquad (1)$$

where M_0 is the long-period seismic moment and τ is the source duration. This formula assumes that the stress drop due to faulting is equal to the effective stress accelerating the fault as it ruptures (Cohn *et al.,* 1982). It is a rough measurement of the stress drop of an earthquake. For the seismic moment, M_0, the moment-magnitude scale $M_0 = 10^{16.1+1.5M_L}$ (Thatcher and Hanks, 1973; Hanks and Kanamori, 1979) has been widely used (e.g., Cohn *et al.,* 1982; Hardebeck and Hauksson, 1996). In this study, we use the seismic moment obtained by grid search, discussed above, and the source duration estimated with Zhao and Helmberger's (1996) method to calculate the relative stress drop with equation (1).

Results

Estimates of the source mechanism, long-period seismic moment, depth, and source duration were obtained for 24 of the best recorded aftershocks. These results are summarized in Table 1. Our depth results are compatible with Hauksson *et al.*'s and are not shown in this table. The source mechanisms are also shown in Figure 8 at the corresponding source locations. In comparison to the two studies mentioned above, our results are closest to those of Hauksson *et al.* (1995). The adjustments are mainly necessary to produce better fit to the Rayleigh waves and to predict better amplitude ratios between the components.

In Figure 9, the seismic moments from this study and those given by Thio and Kanamori (1996) are compared with respect to the local magnitude M_L, given by Hauksson *et al.* (1995). A straight-line moment-magnitude scale ($M_0 = 10^{15.0+1.7M_L}$) for this group of events is also plotted in the same figure. Although these data points follow this scale closer than the well-known Thatcher and Hanks (1973) scale, they fall well in the scatter of the data points for Thatcher and Hanks's (1973) much larger population of southern California earthquakes. In fact, the much larger Northridge mainshock, with $M_0 = (1.4 \pm 0.9) \times 10^{26}$dyne · cm (Song *et al.,* 1995a) and $M_L = 6.7$ (Hauksson

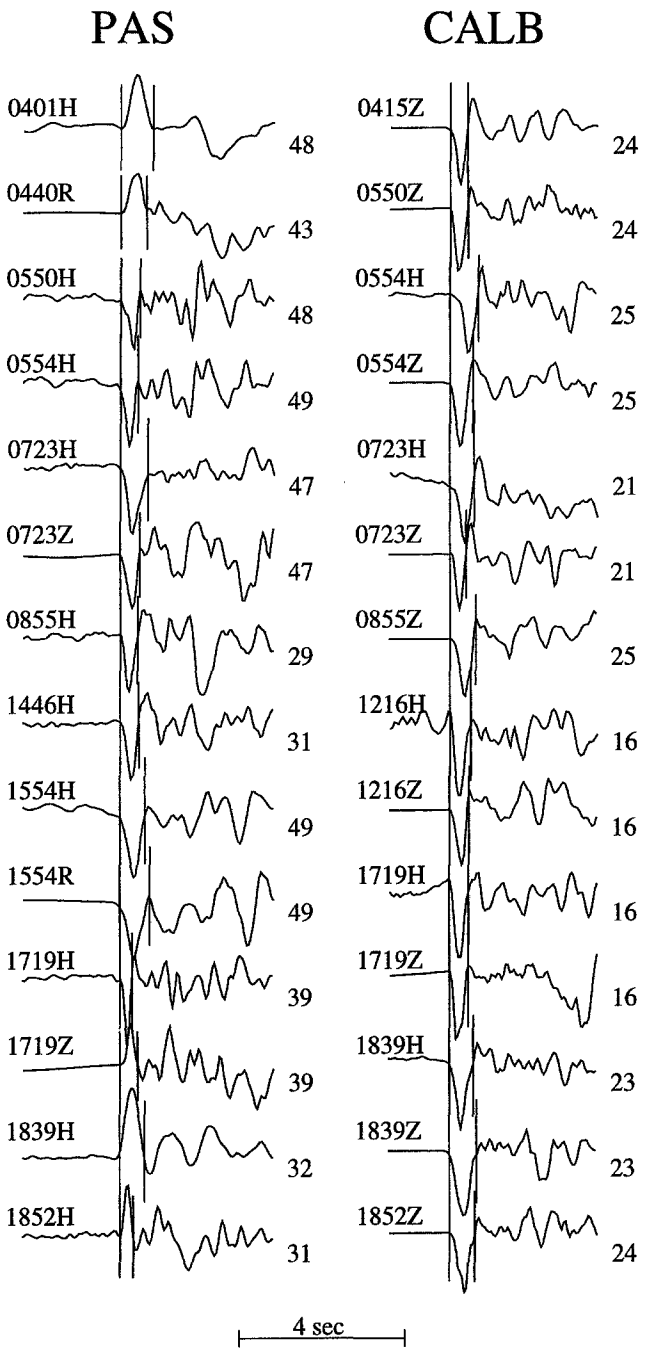

Figure 5. Some of the direct pulses recorded at stations PAS and CALB from which we are able to measure the source duration. Vertical lines indicate the measured duration. Small numbers show source–receiver distances in km. "H", "R," and "Z" following event numbers indicate tangential, radial, and vertical components, respectively.

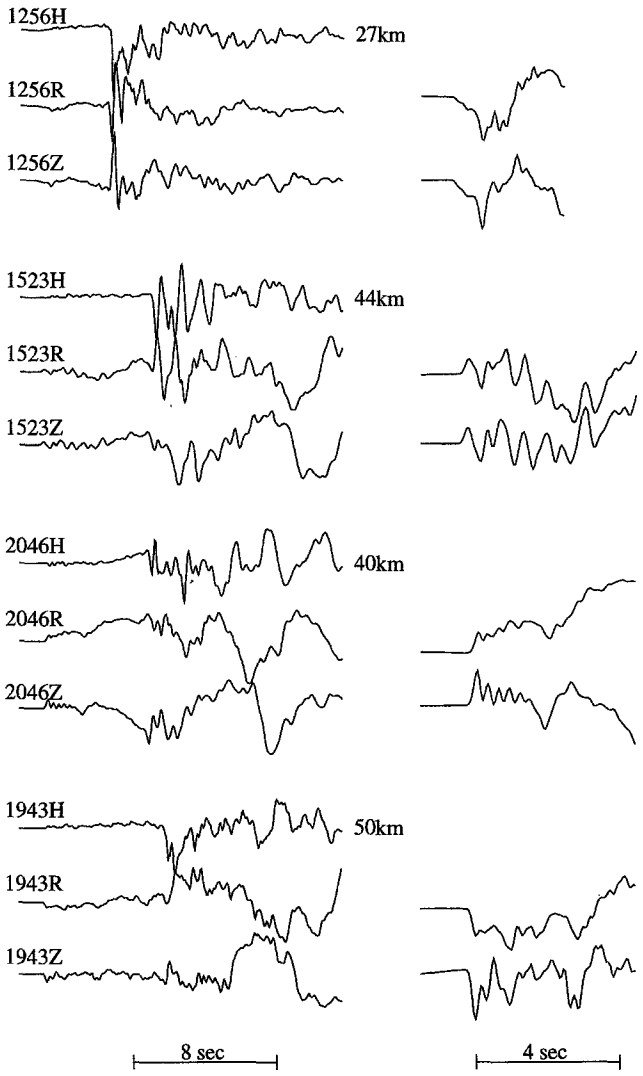

Figure 6. Some of the more complicated records at station PAS, for which direct measurement of the pulse width is difficult. The P_{nl} segment is blown up to the right. Epicentral distances are given.

et al., 1995), falls closer to the Thatcher and Hanks (1973) scale.

Figure 10 shows the distribution of the relative stress drop with respect to the focal depth. Figure 10a uses source depth determined by Hauksson *et al.* (1995). Larger events tend to have higher stress drop compared to small ones. High stress-drop events appear at a depth range of 8 to 15 km. For comparison, in Figure 10b, the same relative stress drop is plotted against the focal depth determined by Mori, who conducted the relocation of these events with a 3D crustal model for the Northridge area (written comm., 1996). The same features are seen, but the high stress-drop zone appears shallower (5 to 13 km).

Discussion and Summary

Throughout this study, we found the Northridge data set to be more complicated than data sets examined in previous TERRAscope studies (e.g., Dreger and Helmberger, 1991; Jones, 1995; Song *et al.,* 1996). The long-period waveform data proved relatively easy to work with, but modeling the broadband data often required special treatment, both in

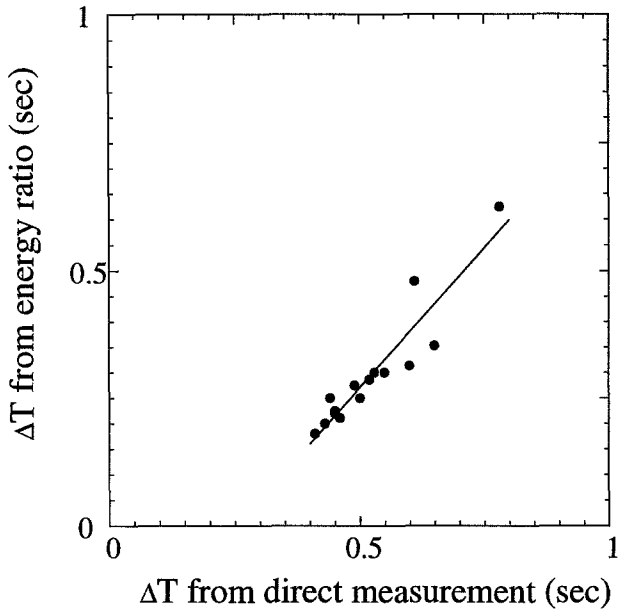

Figure 7. Comparison of two measurements of the source duration of the Northridge aftershocks.

source descriptions and in propagation operators. Figures 11 and 12 show an example (event number 1120) of the more complicated events, modeled as a simple source and as a double event. In Figure 11, we compare the broadband displacement data and the corresponding synthetics determined by the grid-search procedure discussed earlier. Fundamental Rayleigh waves are fit well, but the P_{nl}-wave data are more complicated than the corresponding synthetics. For example, there are obvious secondary pulses in the P_{nl} segment at stations DGR and PFO that do not show up in the synthetics. Note that the separation between these two pulses are approximately the same at stations DGR and PFO, although the distance to these two stations differ by about 50 km.

This suggests a secondary source for this event. In Figure 12, we attempt to model this complexity as a double source, with the far-field source-time function shown at the bottom of the figure. Synthetic waveform fits to the P_{nl} data are improved with this complex source model, but fits to the Rayleigh waves are slightly deteriorated, suggesting that the actual rupture process is more complicated than the simple model we have been assuming.

Severe path effects, such as the San Fernando and the Los Angeles basins, also contribute to the complexity of the Northridge data. As an example, we compare the vertical broadband and short-period displacement data and cumula-

Table 1
Source Parameters for Selected Northridge Aftershocks

Origin Time*			Depth* (km)	M_L^*	θ† (deg)	δ† (deg)	λ† (deg)	$M_0^\ddagger$ (dyne·cm)	$\Delta T_P^\ddagger$ (sec)	$\Delta T_E^\S$ (sec)
940117	1554	10.54	13.3	4.8	30	80	70	1.4e23	0.7	0.35
940117	1756	07.96	19.7	4.6	130	35	100	6.0e22	0.5	0.25
940117	1943	53.17	13.8	4.1	160	80	250	2.4e22		0.35
940117	2046	02.12	10.1	4.9	60	55	10	3.8e23		0.45
940117	2333	30.47	11.1	5.6	120	40	80	9.3e24		1.01
940118	0401	26.03	0.3	4.3	185	55	140	3.1e22	0.8	0.62
940118	0723	55.77	15.9	4.0	90	45	60	2.7e22	0.5	0.30
940118	1523	46.60	9.2	4.8	110	45	80	2.5e23		0.28
940119	0440	47.67	3.1	4.3	315	55	90	3.3e22	0.6	0.31
940119	1409	14.51	18.9	4.5	90	70	80	4.8e22	0.4	0.25
940119	1446	34.96	7.3	4.0	140	50	80	8.4e21	0.5	0.23
940119	2109	28.33	14.3	5.1	95	40	70	1.1e24		0.56
940121	1839	15.05	10.6	4.5	140	40	60	8.5e22	0.6	0.48
940121	1852	44.00	8.9	4.3	90	40	60	2.4e22	0.5	0.21
940123	0855	08.42	9.7	4.1	110	40	80	2.1e22	0.5	0.29
940124	0415	18.55	8.9	4.6	80	55	80	4.8e22	0.4	0.20
940124	0550	24.13	12.1	4.3	110	55	70	2.9e22	0.5	0.22
940124	0554	20.82	10.9	4.2	110	40	70	2.3e22	0.6	0.30
940127	1719	58.58	16.3	4.6	120	10	90	4.3e22	0.4	0.18
940128	2009	53.39	4.0	4.2	140	40	110	1.9e22		0.55
940129	1120	35.60	1.6	5.1	160	65	160	1.5e24		0.81
940129	1216	56.08	3.6	4.3	60	70	10	2.3e22	0.5	0.28
940320	2120	12.03	14.7	5.2	100	40	60	9.9e23		0.41
940525	1256	56.84	11.6	4.4	90	55	75	6.7e22		0.35

*After Hauksson *et al.* (1995).

†θ, strike; δ, dip angle; λ, rake angle; M_0, long-period moment.

‡ΔT_P, source duration measured on TERRAscope stations PAS and CALB.

§ΔT_E, source duration determined by comparing short-period to long-period energy ratio in the data to that in the synthetic.

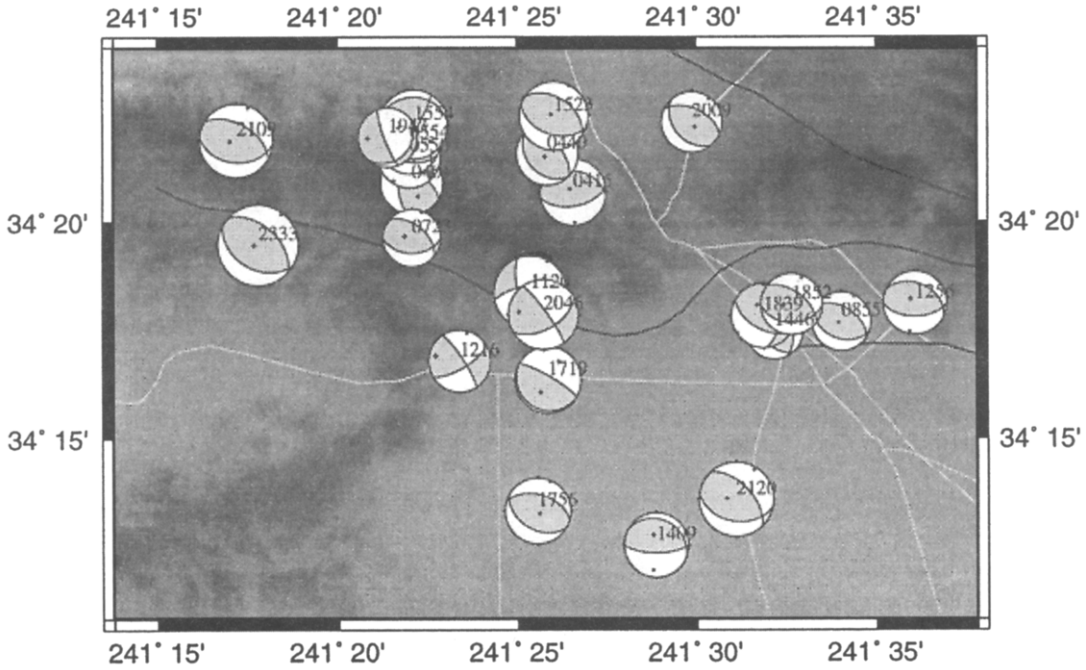

Figure 8. Source mechanisms of the Northridge aftershocks as determined in this study with the grid-search method of Zhao and Helmberger (1994).

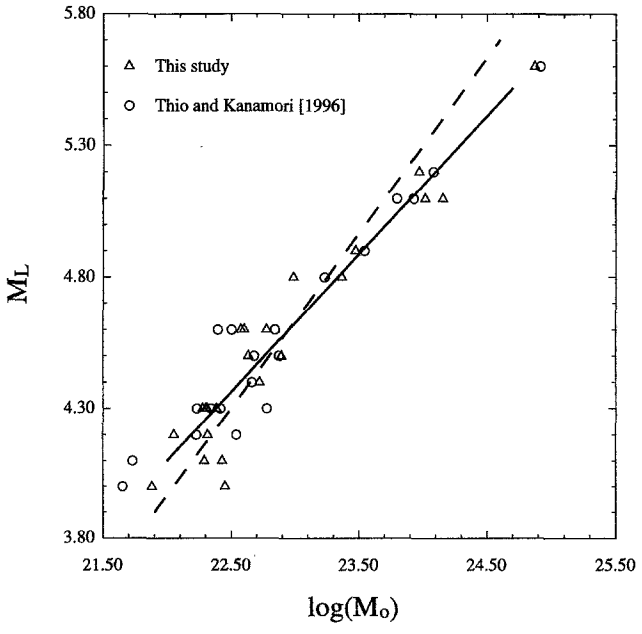

Figure 9. Comparison of long-period seismic moment given in this study and those by Thio and Kanamori (1996), with respect to M_L (Hauksson *et al.*, 1995). The dashed line corresponds to the moment-magnitude scale given by Hanks and Kanamori (1979) for most California events.

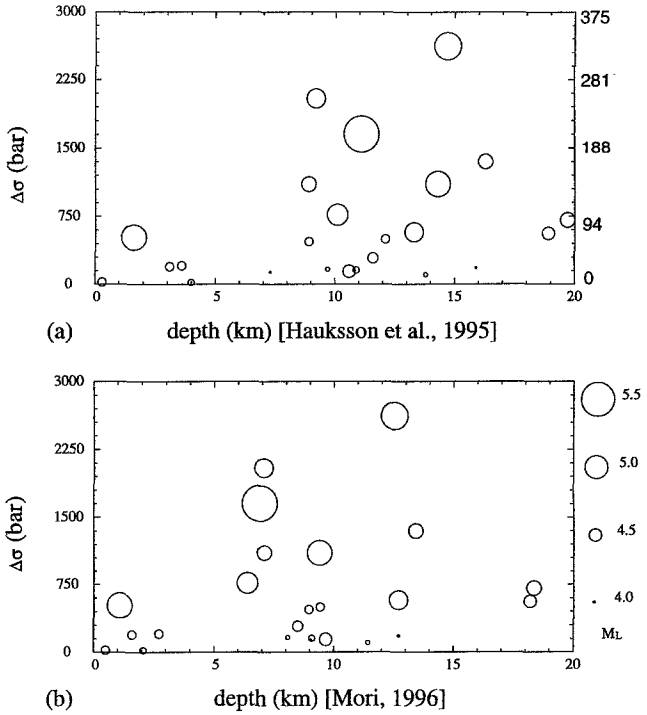

Figure 10. Depth distribution of the relative stress drop for the Northridge aftershocks. Symbol size corresponds to M_L. The stress-drop scale on the right in panel (a) corresponds to the more conventional estimates.

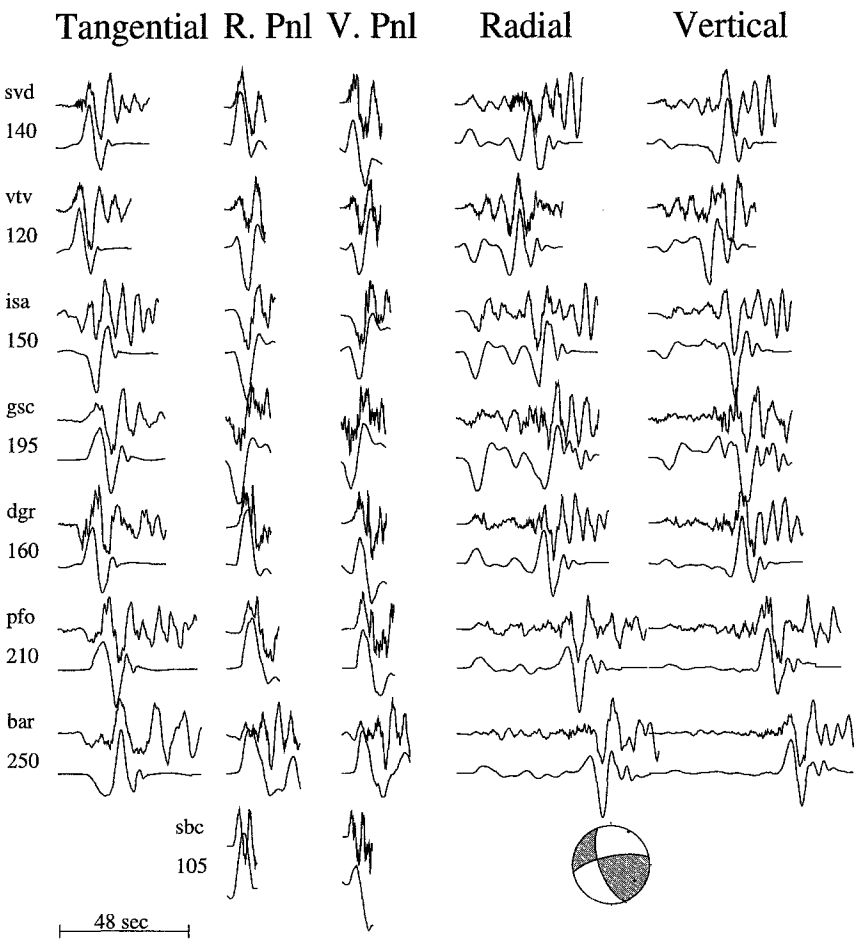

Figure 11. Comparison of broadband displacement data (event 1120) and corresponding synthetics for the mechanism displayed with a trapezoidal far-field source-time function (2.5, 1.8, 2.5 sec) and a source depth of 5 km. All seismograms are scaled to unit height. There is a 40% standard variation for the seismic moment.

tive energy curves for stations GSC and PFO, for three earthquakes at different depths (Fig. 13). These three events occurred under the Santa Susana Mountains within 10 km of each other (Hauksson *et al.*, 1995). Note the difference in the Rayleigh wave train between the records at GSC and PFO for the various events. Seismic signal arrives at station GSC in a time window narrower than at station PFO. This difference is also evident on the short-period records (Fig. 13) but becomes less significant for deeper sources. Scattering due to the more heterogeneous structure from Northridge to PFO could cause this difference. Note that the path from Northridge to station GSC is relatively uniform. The path to PFO traverses the San Fernando basin and part of the Los Angeles basin (Figs. 1 and 8). For a shallow earthquake, part of the surface-wave energy is trapped in the basin and propagates through the slow top layer, producing the extended Rayleigh wave train at station PFO. This could explain the fact that GSC yields a consistently larger seismic moment than does PFO (Fig. 14), since energy, arriving at PFO along different paths, spreads out in a wider time window. Our M_0 estimate is controlled by the amplitude of the first packet of surface-wave energy because the synthetics we used do not include the more dispersed surface wave train. For deep earthquakes, the basin effect is less. However, for the entire group of events, there lacks a clear trend of this complexity with source depth, possibly because of the complex basin structure. To better understand the wave propagation associated with the shallow basins, 2D finite-difference modeling would be helpful, as reported by Song *et al.* (1995b).

Basin effects can also be examined by comparing the ratio of M_e to M_0 for various source depths, averaged over all the network (Fig. 15). M_e^2 is the ratio of the total accumulative energy between data and synthetics, and M_0 is the seismic moment (Zhao and Helmberger, 1996). The M_e/M_0 ratio indicates how much energy is modeled by our 1D synthetics and how much is not, presumably due to the scattering of energy in certain frequency bands by the basin. If the 1D synthetics are efficient in modeling the energy radiation

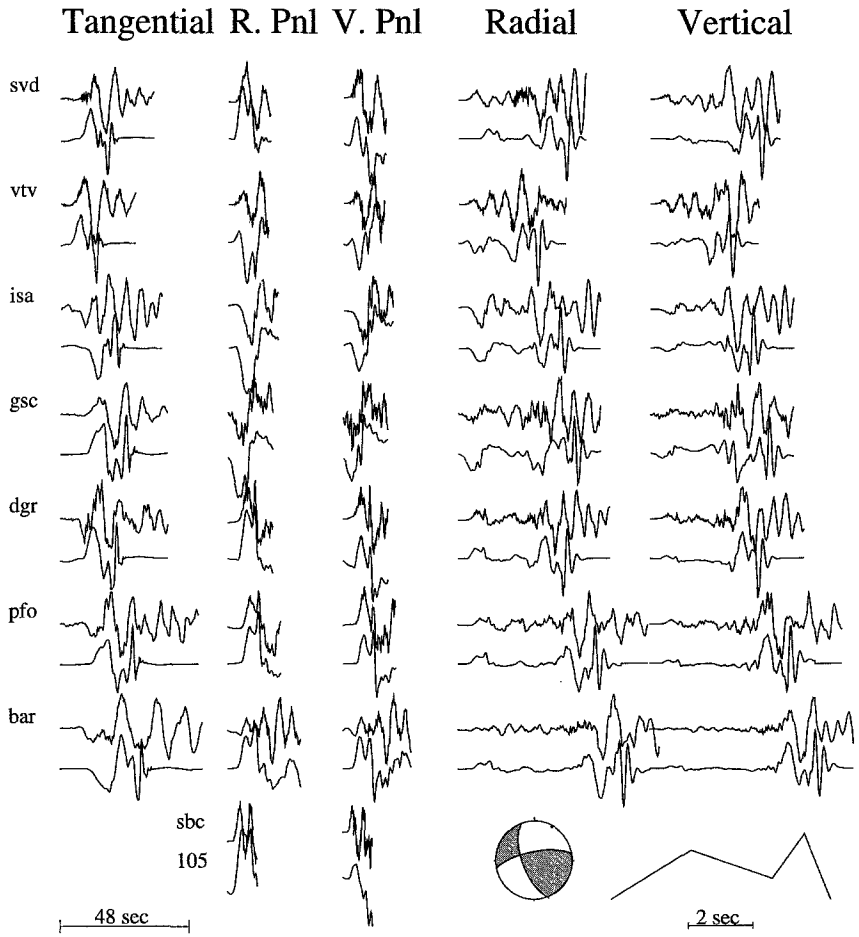

Figure 12. Comparison of broadband displacement data (event 1120) and corresponding synthetics for the mechanism displayed with the far-field source-time function as shown in the lower-right corner and with a source depth of 5 km. Note the improvement in the P_{nl} waveform fit (DGR and PFO) after introducing asperity.

from the source, this ratio should be close to 1. Figure 15a shows the M_e/M_0 ratio in the low-frequency band (LP3090) with respect to source depth for two groups of events: those that are located under the mountains and those under the basin. Note that the average value for the M_e/M_0 ratio is about 1.25, a bias possibly due to the fact that our 1D model is not soft enough at the top. The event with exceptionally high M_e/M_0 ratio is the complex event (number 1120) we discussed above. It occurred near the northwestern edge of the San Fernando basin. Other than this event, there is no obvious depth dependence of the M_e/M_0 ratio. Events under the basin (squares) and those under the mountains (dots) show the same scatter. At short period, some of the shallow events display high M_e/M_0 ratios (e.g., events 1216, 0401, and 1446; Fig. 15b). The scatter is also large, which makes it hard to establish, from this sparse data set, any trend of the M_e/M_0 ratio with respect to the source depth. However, Figure 15b suggests that, among the squares, this ratio can differ by as much as a factor of 3. If scattering at the basin edge is causing this, we would expect, assuming reciprocity, a similar factor from incoming waves, in the event of a regional earthquake occurring outside the basin.

In summary, we studied the TERRAscope waveform data for a set of Northridge aftershocks. Our source mechanisms agree well with focal plots determined from first-motion *P*-wave picks from the Southern California Seismic Network (SCSN) (Hauksson *et al.*, 1995). This result indicates that the longer-period motions associated with surface waves are compatible with the initial rupture motions and that the fault plane does not change appreciably over the rupture history. The same conclusion was also reached in our study of the Northridge mainshock (Song *et al.*, 1995a). Our source depth estimates were determined by the ratio of Rayleigh waves to P_{nl} strengths and generally agree well with Hauksson *et al.* (1995). Since the SCSN array had temporary near-in data for depth control (*S-P* times), we conclude that our independent depth estimates have been validated and should be applicable for events in other regions where near-in data are not available. Source duration was estimated by comparing short- to long-period energy ratio

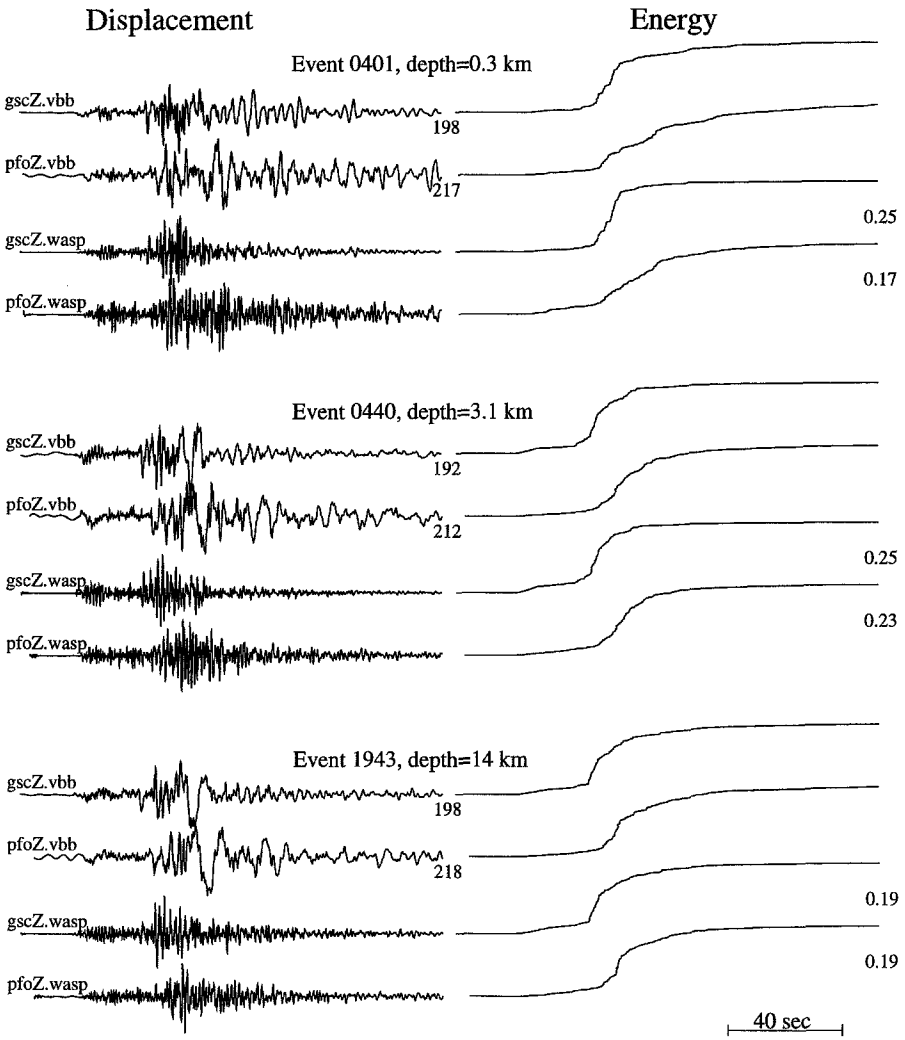

Figure 13. Comparison of the broadband and short-period (WASP) vertical displacement data and cumulative energy curves for stations GSC and PFO for three Northridge aftershocks at different depths. In the displacement columns, numbers indicate epicentral distances. In the energy column, the short-period to broadband energy ratios are shown for each record. Note the degree of complexity as a function of source depth and station.

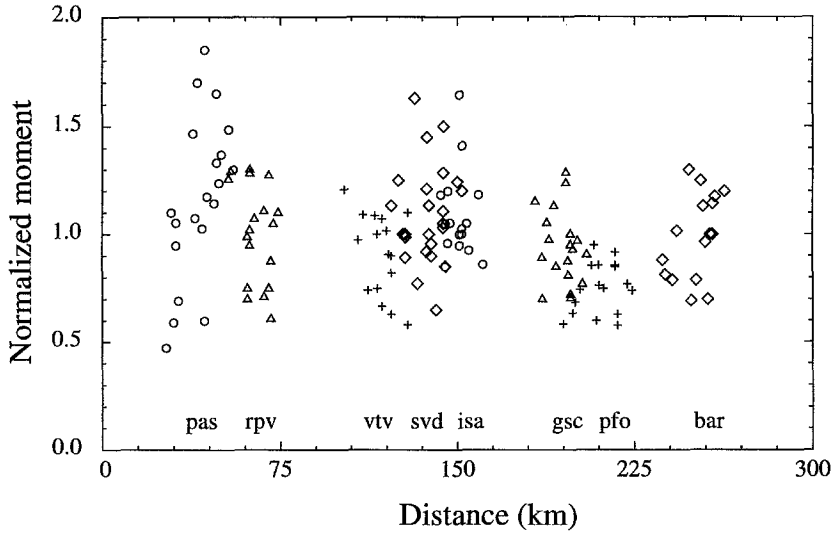

Figure 14. Display of single-station moment estimates normalized by the average value over TERRAscope, for the Northridge aftershocks. Note that stations PAS and SVD display the largest scatter. Station GSC yields consistently larger moment than PFO.

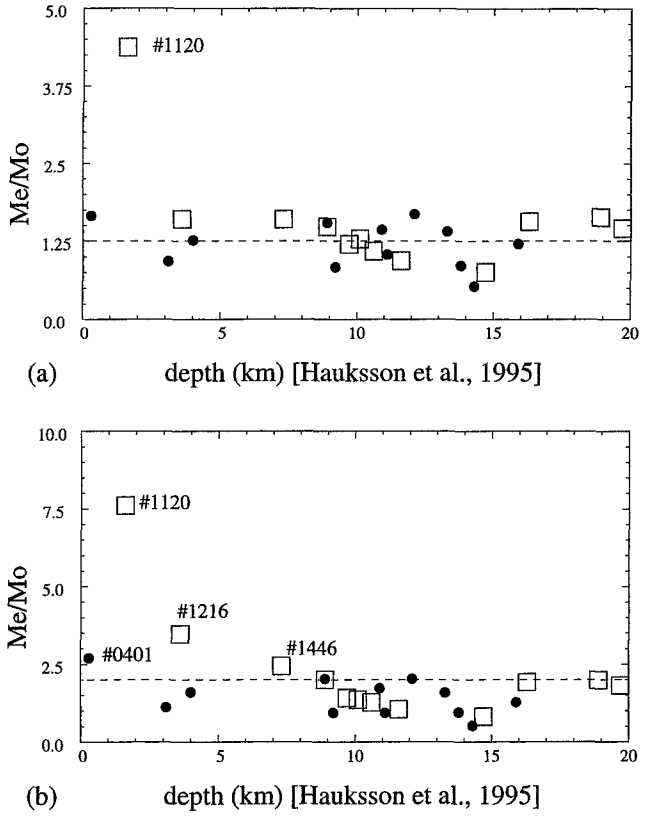

Figure 15. M_e/M_0 ratio of Northridge aftershocks with respect to focal depths by Hauksson *et al.* (1995): (a) in low-frequency band (LP3090) and (b) in high-frequency band (WASP). Black dots correspond to events under the mountains. Squares correspond to events under the San Fernando basin. Vertical components at stations BAR, GSC, ISA, PAS, PFO, RPV, SVD, and VTV are used to calculate M_e.

in the P_{nl} data, relative to synthetics. This method, originally proposed by Zhao and Helmberger (1996), was tested against the more traditional method of measuring the width of direct pulses and proved to be an effective means of modeling broadband seismograms and providing consistent source duration estimates. Stress drop of the aftershocks were calculated using these estimates and their depth distribution indicates a zone of high relative stress drop at the depth range of 5 to 15 km, with the larger events yielding the highest stress drops.

Acknowledgments

We thank the Data Center of the Southern California Earthquake Center for making the Northridge data set available. Katrin Hafner helped us in retrieving these data. Craig Scrivner, Andy Michael, Jeroen Ritsema, and Lind Gee provided critical reviews along with very helpful suggestions. This research was supported by SCEC under Contract Number 569933, as funded by NSF Number 89-20136 and USGS Number 1434-93-G-2322. Contribution Number 5653, Division of Geological and Planetary Sciences, California Institute of Technology, Pasadena, California.

References

Bouchon, M. (1981). A simple method to calculate Green's functions for elastic layered media, *Bull. Seism. Soc. Am.* **71,** 959–971.

Cohn, S. N., T.-L. Hong, and D. V. Helmberger (1982). The Oroville earthquakes: a study of source characteristics and site effects, *J. Geophys. Res.* **87,** no. B6, 4585–4594.

Dreger, D. (1992). Modeling earthquakes with local and regional broadband data, *Ph.D Thesis,* California Institute of Technology, Pasadena, California.

Dreger, D. and D. V. Helmberger (1991). Source parameters of the Sierra Madre earthquake from regional and local body waves, *Geophys. Res. Lett.* **18,** no. 11, 2015–2018.

Fuchs, K. and G. Müller (1971). Computation of synthetic seismograms with reflectivity method and comparison with observations, *Geophys. J. R. Astr. Soc.* **23,** 417–433.

Hanks, T. C. and H. Kanamori (1979). A moment magnitude scale, *J. Geophys. Res.* **84,** 2348–2350.

Hardebeck, J. and E. Hauksson (1996). Patterns of stress drop in the 1994 Northridge aftershock sequence, *Bull. Seism. Soc. Am.* (submitted).

Hauksson, E., L. M. Jones, and K. Hutton (1995). The 1994 Northridge earthquake sequence in California: seismological and tectonic aspects, *J. Geophys. Res.,* **100,** 12335–12355.

Jones, L. E. (1995). Broadband modeling of aftershocks from the Joshua Tree, Landers, and Big Bear sequences, southern California, *Ph.D Thesis,* California Institute of Technology, Pasadena, California.

Jones, L. E. and D. V. Helmberger (1996). Seismicity and stress-drop in the eastern Transverse ranges, southern California, *Geophys. Res. Lett.* **23,** no. 3, 233–236.

Saikia, C. K. (1994). Modified frequency-wavenumber algorithm for regional seismograms using Filon's quadrature-modeling of Lg waves in North America, *Geophys. J. Int.* **118,** 142–158.

Song, X. J., L. E. Jones, and D. V. Helmberger (1995a). Source characteristics of the 17 January 1994 Northridge, California, earthquake from regional broadband modeling, *Bull. Seism. Soc. Am.* **85,** 1591–1603.

Song, X. J., C. W. Scrivner, and D. V. Helmberger (1995b). Source characteristics of Northridge aftershocks, with application to the effect of San Fernando Basin on the propagation of seismic energy, *EOS* **76,** no. 46, F356.

Song, X. J., L. Zhao, and D. V. Helmberger (1996). Broadband modeling of regional seismograms; the Basin and Range crustal structure, *Geophys. J. Int.* **125,** 15–29.

Thatcher, W. and T. C. Hanks (1973). Source parameters of Southern California earthquakes, *J. Geophys. Res.* **78,** 8457–8576.

Thio, H.-K. and H. Kanamori (1995). Moment tensor inversion for local earthquakes using surface waves recorded at TERRAscope, *Bull. Seism. Soc. Am.* **85,** 1021–1038.

Thio, H.-K. and H. Kanamori (1996). Source complexity of the 1994 Northridge earthquake and its relation to aftershock mechanisms, *Bull. Seism. Soc. Am.* **86,** S84–S92.

Zhao, L. and D. V. Helmberger (1994). Source estimation from broadband regional seismograms, *Bull. Seism. Soc. Am.* **84,** 91–104.

Zhao, L. S. and D. V. Helmberger (1996). Regional moments, energy levels, and a new discriminant, *Pure Appl. Geophys.* **146,** 281–304.

Zhu, L. and D. V. Helmberger (1995). Advancement in source estimation techniques using broadband regional seismograms, *EOS* **76,** no. 46, F424.

Seismological Laboratory
California Institute of Technology
Pasadena, California 91125

Manuscript received 3 October 1996.